Laser Chem. Vol. 7, pp. 305–331

Printed in the United Kingdom

Multiphoton Absorption of $^{12}CF_3I$, $^{13}CF_3I$, CF_3Br and SF_6 by a High Pressure CO_2 Laser

C. ANGELIÉ, R. CAPITINI and P. GIRARD

C.E.A.-I.R.D.I., Département de Physico-Chimie, Centre d'Études Nucléaires de Saclay, 91191 Gif-sur-Yvette Cedex, France

(Received August 1, 1986; in final form December 18, 1986)

An investigation of the IR multiphoton absorption (MPA) of $^{12}CF_3I$, $^{13}CF_3I$, CF_3Br and SF_6, excited in cell by a 10 Bars TE CO_2 laser is reported. The spatial, spectral and temporal characteristics of the laser emission versus the grating position have been carefully investigated. The main result is that the peaks observed in the different MPA spectra are undoubtedly correlated to the gain curve of the laser and not to the fine molecular spectroscopy.

This result is discussed in comparison with published similar works. The most likely explanation involves a laser bandwidth effect associated with a background of weak but rather dense resonances (typical spacing of 0.1–0.2 cm^{-1}). The MPA cross section of $^{13}CF_3I$ is about half that of $^{12}CF_3I$ pointing out the probable rôle of Fermi resonances.

KEY WORDS: Multiphoton absorption, CO_2 lasers, Fermi resonances, SF_6 spectra.

1. INTRODUCTION

Since the discovery of the IR multiphoton absorption (MPA) process of polyatomic molecules and of its isotopic selectivity, the understanding of its mechanism has been improved by investigations in different experimental directions. Particularly, multiatmospheric CO_2 lasers[1,9] are very promising because they allow a continuously tunable excitation over ranges of several tens of cm^{-1}, with a typical resolution of 0.1 cm^{-1}, while TEA lasers provide only discrete lines spaced of

1.8 cm^{-1} (P branch) or 1.2 cm^{-1} (R branch). Such an excitation source can be suitable to point out the rovibrational steps which play an important rôle in the MPA process of a given molecule, at least up to the so-called quasi-continuum which seems to set up near 4000 cm^{-1} for SF_6 and 6000 cm^{-1} for $^{12}CF_3I$.[10]

However, the MPA process is far from being completely and quantitatively understood. One reason of this situation is that experimental improvements in one direction are generally insufficient to state clearly the relevant mechanisms. It is particularly the case for high pressure CO_2 laser experiments, for which the continuous tunability is obtained at the prejudice of the control of spatial and spectral characteristics, if no selective element other than the grating is introduced in the cavity. We have experimentally and theoretically investigated these laser characteristics elsewhere.[11]

In this paper we have carefully examined the MPA spectra of various molecules: $^{12}CF_3I$, $^{13}CF_3I$, CF_3Br, SF_6, measuring systematically the characteristics of the 10 Bars CO_2 laser emission. The comparison between $^{12}CF_3I$ and $^{13}CF_3I$ is of particular interest to point out the rôle of Fermi resonances.[12]

2. EXPERIMENTAL RESULTS

2.1. Laser characteristics

The high pressure TE CO_2 laser (HPL) is a Lumonics 281. Unless stated, it is used with an intracavity pressure of 10 Bars. It is essential for the optical frequency stability that the gas flow be regular and the external pressure set about 2 Bars above the cavity one. The laser operates with a 84/8/8 $He/CO_2/N_2$ mixture. The Ge output coupler has a 65% reflectivity and the grating has 135 lines/mm. The gas cavity is limited by NaCl Brewster windows. An inside cavity diaphragm of 8 mm diameter allows a quasi TEM_{oo} beam. The cavity length is 108 cm and the active volume is 66 cm long. The repetition rate is set at 0.5 Hz. The maximum output energy is limited to 300 mJ to avoid excessive optical damages.

Detailed measurements of the emission characteristics have been reported in Ref. 11. We give here the main results obtained. First, the spatial distribution of the beam was studied with a small pinhole 4 m

after the output coupler. In the 10*P* 24 line center, the distribution is quasi-gaussian with a full width of 7.4 mm at the 1/e intensity point (f.w. 1/e). For an incident energy of 70 mJ at the cell entrance, this width corresponds to a maximum fluence ϕ of 170 mJ/cm^2. In the 10*P* 22–24 CO_2 gain minimum, the spatial profile was found distorted, with a quasi-trapezoidal shape and a f.w. 1/e of 9.5 mm, while the profile center was shifted of 1.5 mm. For the incident energy of 70 mJ, the maximum fluence ϕ was reduced to 110 mJ/cm^2. Then, the spatial profile is modulated versus the gain curve of the gas mixture.

Second, the spectral distribution was scanned versus the grating position x with an optical multichannel analyzer (OMA) from EGG/PAR, coupled with a Jobin-Yvon monochromator. The instrumental resolution γ_i measured with a single longitudinal mode cw CO_2 laser (SAT, model C7) is 80.10^{-3} cm^{-1}. The frequency calibration of the OMA was obtained by means of the CO_2 discrete lines emitted by the HPL operating at 2 Bars. The laser line center is noted $C(x)$ for a given grating position. The laser linewidth $\gamma_L(x)$ is computed from the measured linewidth γ_m by using $\gamma_L = \sqrt{\gamma_m^2 - \gamma_i^2}$. It is convenient to correlate the spectral characteristics to the CO_2 gain curve. For this purpose, we have plotted the responsivity curve $R(x)$ of the laser emission, defined step to step by the output energy variations when the grating position x is scanned.

The maxima of the $R(x)$ curve are normalized to 100. In Figure 1, we have reported the results obtained between the 10 P 18 and 10 P 24 lines: the curves $C(x)$, $R(x)$, $\gamma_m(x)$ (in OMA channels), $\gamma_L(x)$ (10^{-3} cm^{-1} unit) are plotted. The curve $C(x)$ exhibits a slight oscillation around a straight line: it is the frequency pulling effect. Its amplitude is ± 0.11 cm^{-1}. The curve $R(x)$ reflects well the CO_2 gain curve with, however, a slight shift of the maxima of $+0.15$ cm^{-1}. This is likely due to a slight asymmetric collimation introduced in the laser cavity by the Brewster windows. After the shift correction of 0.15 cm^{-1} and the frequency pulling correction, the $R(x)$ curve allows a frequency calibration with an accuracy of ± 0.07 cm^{-1}. The curve $\gamma_L(x)$ shows a strong modulation correlated to the CO_2 gain curve: the linewidth is broadened from 70–100 10^{-3} cm^{-1} in the gain maxima to 200 10^{-3} cm^{-1} in the gain minima. Moreover, the spectral distribution is split in two distinct lines distant of about 0.15 cm^{-1} for several x positions near the gain minima. In this case, the linewidth reported is the sum of each peak linewidth and there are two points on the $C(x)$ curve for a given x

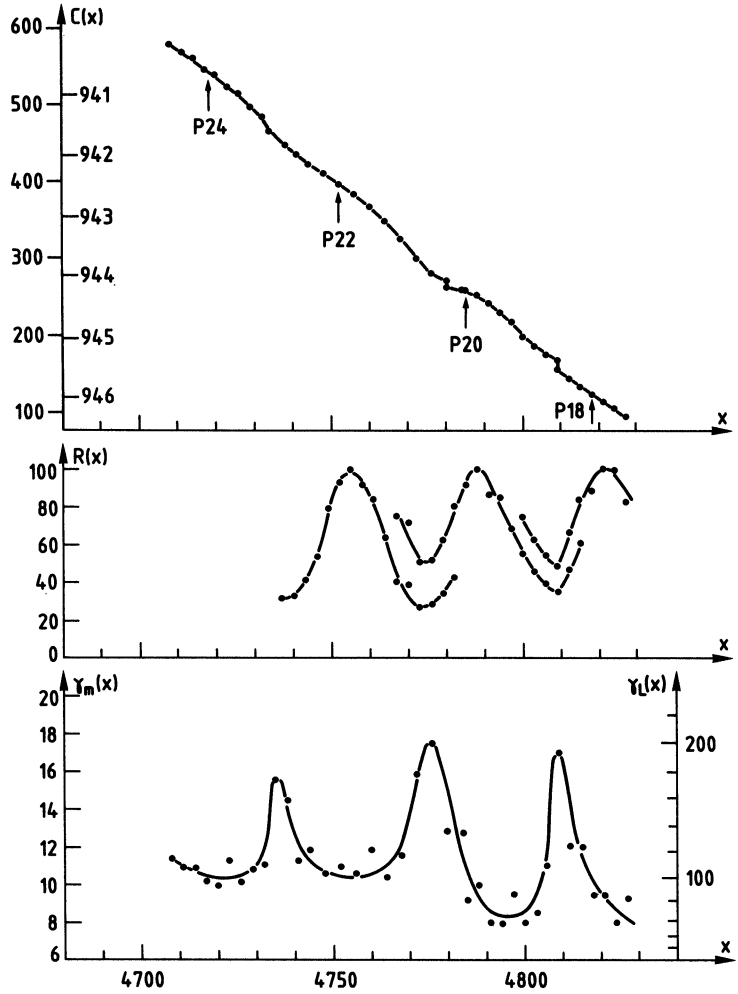

Figure 1 Spectral characteristics of the high pressure CO_2 laser between $10P$ 18 and $10P$ 24 lines. x: grating graduation; C: line center position in OMA channels (left scale) and cm^{-1} (right scale); γ_m: measured f.w.h.m. spectral linewidth in OMA channels; γ_L: deconvoluted f.w.h.m. laser linewidth in 10^{-3} cm^{-1}; $R(x)$: responsivity curve, reflecting the gain curve (see text; maxima are normalized to 100). CO_2 discrete line centers are indicated by an arrow.

grating position. The linewidth was also measured at 1% of the maximum, with a 40 pulses accumulation, giving 0.21 cm^{-1} in the 10*P* 22 line center and 0.43 cm^{-1} in the 10*P* 22–24 gain minimum.

The theoretical model of the spectral distribution of high pressure CO_2 lasers developed in Ref. 11 explains quantitatively the simultaneous spatial distortion and broadening or splitting of the lines in the gain minima.

Finally the temporal shape of the pulses was observed, for an output energy of 200 mJ, with a 1 ns resolution by using a photon drag. The peak has a 45 ± 10 ns duration f.w.h.m. without tail and exhibits partial self-mode-locking occurring in a random way. No difference was noted from gain maxima to gain minima around 10*P* 22 or 10*P* 24 lines.

2.2. Experimental device of multiphoton absorption. Measurement methods

The experimental device is shown in Figure 2. A removable beam splitter L_1 allows a rough determination of the wavelength on the spectrum analyzer (S.A.) from Optical Engineering Inc. A 10% reflective beam splitter L_2 directs a beam part on a pyroelectric detector (model LED 200C from Gen Tec). Unless stated, the laser output energy is set to 250 mJ. The beam is divided on a 35% reflective beam splitter L_3. The transmitted part is directed towards the first probe S_1 of the ratiometer via the mirrors M_2 and M_3. The reflective part of 70 mJ enters a cell 40 cm long closed with KCl windows. The pressure is monitored with a Barocel pressure sensor from Datametrics and the possible dissociation of molecules is controlled by a double beam IR spectrometer Perkin-Elmer 281. At the end of all the experiments no dissociation was observed within 2% of the initial pressure and no correction of the data is necessary. After the cell, the beam is directed towards the second probe S_2 via the mirror M_4. S_1 and S_2 are RjP 734 pyroelectric probes, connected to a Rj 7200 energy ratiometer manufactured by Laser Precision Corporation. The probes were shielded and the ratiometer ground $G2$ was electrically isolated from the laser ground $G1$. We have chosen for the absorption measurements the most direct method, i.e. a double ratiometric measurement for each grating position x. The detailed procedure is the following: the cell is filled once for all with a given gas pressure. The

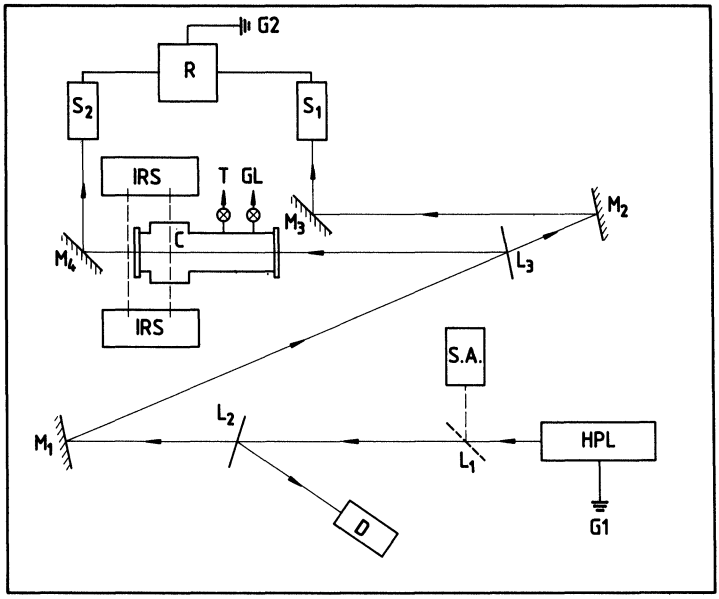

Figure 2 Experimental device. HPL: high pressure TE CO_2 laser; S.A.: spectrum analyzer; L_1: removable beam splitter; L_2: 10% reflective beam splitter; D: pyroelectric detector; M_1, M_2, M_3, M_4: plane mirrors; L_3: 35% reflective beam splitter; C: cell; G.L.: to the gas line; T: trapping in liquid nitrogen; I.R.S.: double beam I.R. spectrometer; S_1, S_2: pyroelectric probes; R: ratiometer; G_1, G_2: electrical grounds.

grating position x is fixed. The intensity ratio ρ_f of the beam directed on the probes S_2 and S_1 is measured for the filled cell over 80 pulses. Then the gas is trapped at the liquid nitrogen temperature and the intensity ratio ρ_e for the empty cell is measured again over 80 pulses.

The appropriate quantity is the measured absorbance A_m defined by:

$$A_m = -\mathrm{Ln}\ (\rho_f/\rho_e)$$

It is important to note that the gas is not changed during all the experiment. The absolute accuracy on A is $\pm 1\%$. As previously mentioned, the laser gas flow must be regular and more generally, the laser must be in permanent working condition to ensure the accuracy of the measurements and avoid frequency jumps which can be responsible for non significant structures in the absorption spectrum. The true

molecular absorbance is noted A and gives a gas transmission factor e^{-A}. A is related to an average MPA cross section $\langle\sigma\rangle$ by:

$$A = nl\,\langle\sigma\rangle$$

(for a cell length l). The cross section $\langle\sigma\rangle$ is averaged over the entire cell volume, according to:

$$\langle\sigma\rangle = \frac{1}{l}\int_0^l dl\left[\int dS\,\sigma\phi \Big/ \int dS\,\phi\right] \tag{1}$$

where dS is a surface element of each cell section, σ and ϕ respectively the MPA cross section and the fluence (in J/cm^2) at each point of the cell. Obviously, if σ is independent of ϕ: $\langle\sigma\rangle = \sigma$. The average number $\langle p\rangle$ of photons absorbed for a given fluence ϕ can be computed from A using:

$$\langle p\rangle = \frac{A\phi}{nlh\nu} \tag{2}$$

The input energy was fixed to 70 mJ at the cell entrance. Due to the spatial deformation previously mentioned this constant energy corresponds to a fluence varying from 110 to 170 mJ/cm^2 and $\langle p\rangle$ has been computed for a standard ϕ value of 140 mJ/cm^2.

The relation between the measured absorbance A_m and the true gas absorbance A can be expressed as following: let T_{2f} be the fraction of the laser pulse energy transmitted towards the probe S_2 by the different optical elements, gas excepted, when the cell is filled, and T_{2e} this fraction when the cell is empty:

$$A_m = A - \mathrm{Ln}\,(T_{2f}/T_{2e}) \tag{3}$$

T_{2f} and T_{2e} can depend on x and on the fluence through the different optical elements. However, if the presence of the gas does not modify the transmittance of these optical elements through, for example, the intensity variation, $A_m = A$. This point will be discussed later.

2.3. Multiphoton absorption spectra at 10 Bars

The first molecule studied is $^{12}CF_3I$. The MPA spectrum is reported in Figure 3 from 1068.5 to 1085.5 cm^{-1} for a pressure of 0–400 mBar. The

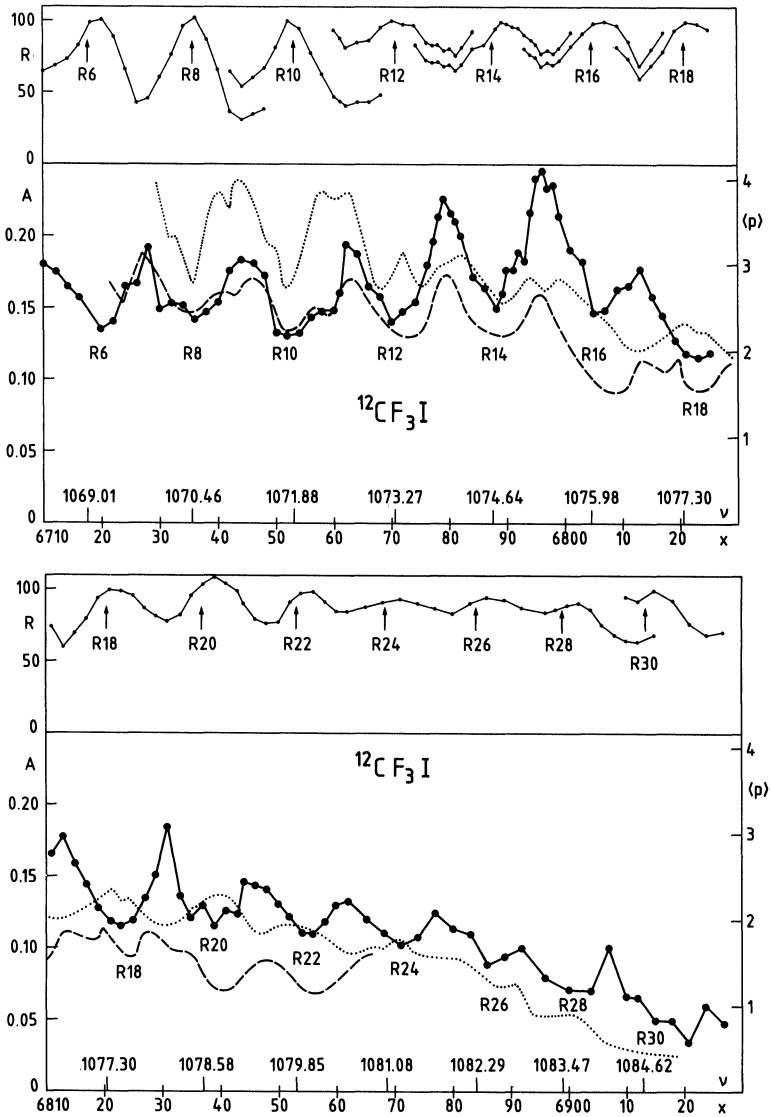

Figure 3 $^{12}CF_3I$ MPA spectrum at 0.400 mBar and 70 mJ input energy; laser cavity pressure: 10 Bars; 9*R* branch; *x*: grating graduation; *ν*: optical frequency in cm^{-1}; *A*: absorbance; $\langle p \rangle$: average number of photons absorbed, computed for an average fluence of 140 mJ/cm^2; *R*: responsivity curve (similar to CO_2 gain curve, see text). The spectra of Refs. 5 (dotted line) and 9 (dashed line) are plotted for comparison.

responsivity curve is shown above the spectrum. The absorbance is maximum around the ν_1 mode (1075.2 cm^{-1}) and, for $\phi = 140\,mJ/cm^2$, the average number of photons absorbed is 4.1. The absorption decreases slowly for lower frequencies and faster for greater frequencies. The main feature is a striking correlation between the MPA spectrum and the responsivity curve: the absorption maxima are undoubtedly corresponding to the minima of the CO_2 gain curve and vice versa. The spectra of Refs. 5 (dotted line) and 9 (dashed line) are shown for comparison and will be discussed in the next section.

The second molecule studied is $^{13}CF_3I$ which has been enriched by us from the natural $^{12}C/^{13}C$ mixture by using selective multiphoton disso-

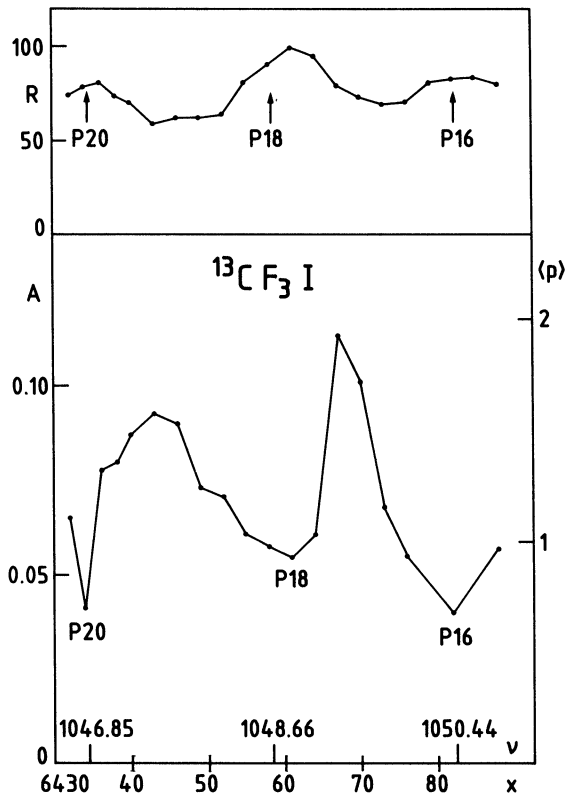

Figure 4 $^{13}CF_3I$ MPA spectrum at 0.400 mBar in the 9*P* branch. For other data see Figure 3.

ciation of $^{12}CF_3I$ and separation of C_2F_6 by distillation at $-145°C$ with isopentane[13]. The enriched product contained 95% of $^{13}CF_3I$, the remaining being $^{12}CF_3I$ and a small proportion of C_2F_6. A small part of the spectrum around the ν_1 mode (1047.6 cm^{-1}) has been explored for a pressure of 0.400 mBar and an input energy of 70 mJ (Figure 4). The absorbance shows the same modulation correlated to the CO_2 gain curve. Another interesting result is that the maximum absorbance

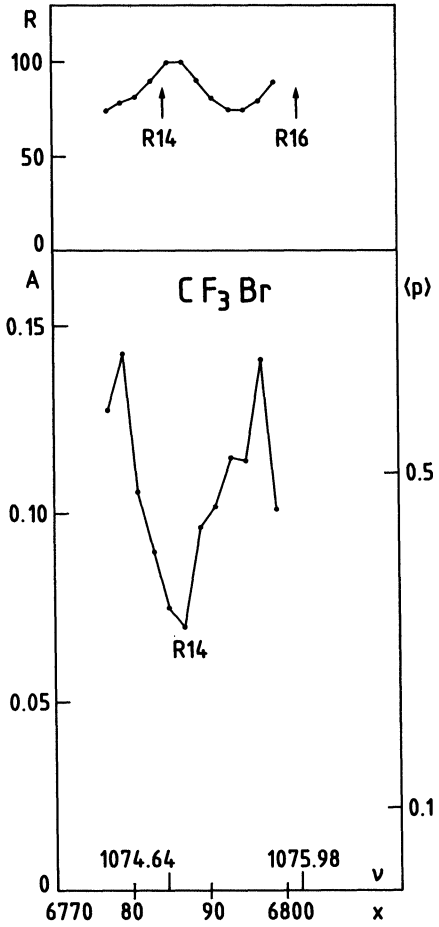

Figure 5 CF_3Br MPA spectrum at 1.48 mBar in the 9*R* branch. For other data see Figure 3.

peak near the ν_1 frequency is only 0.124 i.e. about half the value obtained for $^{12}CF_3I$ around its ν_1 mode for the same pressure and energy.

A small part of the CF_3Br natural isotopic mixture (^{79}Br: 50.5%, ^{81}Br: 49.5%) has been recorded at a pressure of 1.48 mBar, and an input energy of 70 mJ. The curves are plotted in Figure 5. The same correlation between absorbance and responsivity is observed. The maximum number of photons absorbed is 0.63.

Finally, a part of the SF_6 spectrum has been explored at a pressure of 0.400 mBar and an input energy of 70 mJ, confirming the correlation. The maximum number of photons absorbed is 6.5 (Figure 6). A part of the spectrum of Ref. 1 (reported in arbitrary unit) is also shown. It has been obtained at 140 K and the range explored extends out off our one.

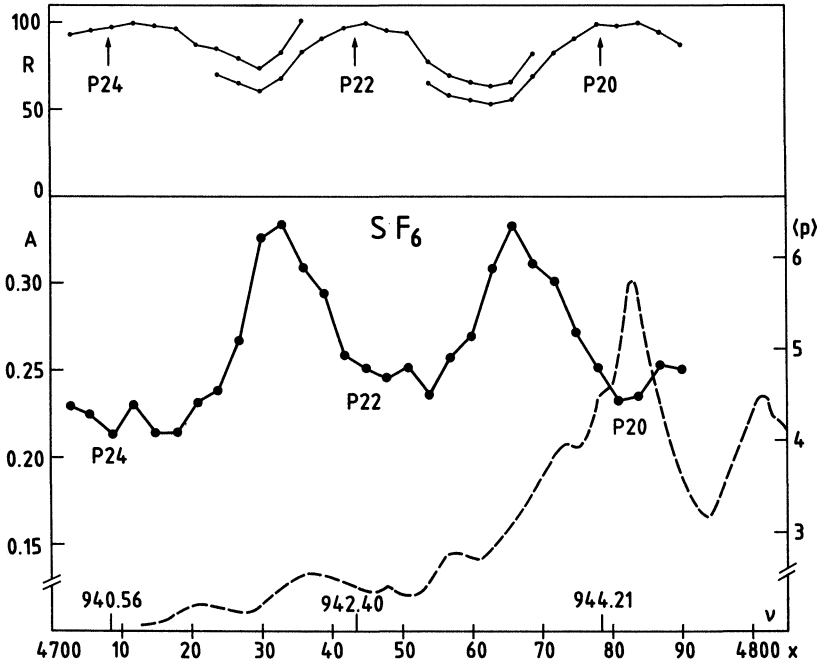

Figure 6 SF_6 MPA spectrum at 0.400 mBar in the 10*P* branch. For other data see Figure 3. A part of the spectrum of Ref. 1 is plotted for comparison (dashed curve).

2.4. Complementary experiments

Several explanations of this striking correlation can be invoked: a laser spectral bandwidth effect analogous to that of Ref. 4; a modulation of the time-intensity distribution at constant fluence; a consequence of the spatial deformation; or an artefact due to the experimental device. In order to understand the mechanism responsible for the correlation observed, several complementary experiments have been performed.

a) The energy dependence of the absorbance has been measured for the SF_6 molecule. In the $10P$ 22 line center, when the laser energy varies from 295 to 50 mJ, the absorbance varies between 0.204 and 0.221 without any systematic tendency and within the experimental accuracy. In the $10P$ 24–22 gain minimum for the same energy variations, the absorbance is varying between 0.305 and 0.327. Then, the absorbance can be considered as energy independent around the $10P$ 22–$10P$ 24 lines. This result is also valid for $^{12}CF_3I$ around the $9R$ 18 line.

Moreover, it was observed that when the intensity is divided by 2, the window transmission is only reduced by 3%.

b) The pressure dependence has been examined for SF_6. When the pressure varies from 0.400 to 0.130 mBar, the pressure dependence can be expressed by a $P^{0.97\pm0.10}$ law in the $10P$ 24 line center and by $P^{1.15\pm0.10}$ in the $10P$ 22–24 gain minimum. The same approximate proportional law is also valid for $^{12}CF_3I$.

c) The possible rôle of spatial distortions has been studied shifting slightly by about ±5 mm the beam position relatively to the cell or the probes: no effect was noticed, as expected for a double ratiometric method. A diaphragm of 8 mm diameter was also placed outside the laser: a small diminution of the absorbance seems to be observed but far from the modulation reported: for SF_6 in the $10P$ 24 line center, A varies from 0.345 without diaphragm to 0.321 with diaphragm. In the $10P$ 22–24 gain minimum, the respective values are: 0.247 and 0.226.

d) In view of eliminating possible artefacts such as ratiometer or probes disturbances, self focusing or defocusing effect by the gas,[14,15] absorbance measurements have been performed again with a single detector placed successively before and after the cell, near the windows, and with sufficient average (8 series of 10 pulses). Several points have been checked and the previous results were always confirmed.

The effect of the laser characteristics has been further examined by varying several parameters.

e) In view of a better understanding of the laser gain rôle, the laser pressure has been fixed to 5 Bars and a small part of the $^{12}CF_3I$ MPA spectrum has been plotted again with a simultaneous monitoring of the wavelength λ (Figure 7). The maximum absorbance is slightly attenuated from 0.24 to 0.21 but the absorbance or responsivity curves are similar to the Figure 3 curves. However, this similarity masks strong differences of the $\lambda(x)$ curve: $\lambda(x)$ was nearly linear at 10 Bars while, at 5 Bars it jumps from one line center to the next.

f) The inside cavity diaphragm was set from 8 to 12 mm. It has been shown in Ref. 11 that such a modification enhances considerably the broadening and splitting of the laser spectral emission in the gain minima giving 3 peaks with a spacing of $0.43\,cm^{-1}$ between adjacent peaks. The sum of the partial linewidths is $0.40\,cm^{-1}$. However, measurements for SF_6 at the $10P$ 24 line center and in the $10P$ 22–24 gain minimum shows no significant variation of the absorbance within $\pm 1\%$.

g) The laser pressure was also varied from 10 Bars to 2 Bars for a given line center, but the input energy could not exceed 15 mJ (30 mJ/cm^2). For SF_6 at the $10P$ 24 line center or $^{12}CF_3I$ at the $9R$ 18 line center, no significant difference has been observed in spite of the reduction of the laser bandwidth from 70–100 10^{-3} cm^{-1} to about 30 10^{-3} cm^{-1}.

h) Finally, the grating, the output coupler and the Brewster windows have been replaced and several values checked: the previous results were again confirmed showing that the correlation is not due to a particular parasitic characteristic of the laser such as damages on some optical element.

2.5. Analysis of experimental data

Before discussing the fundamental implications of the previous results it is necessary to examine their meaning. The relation between A_m and A is given by (3). As experimentlly observed, the transmission factor T_2 is diminished by about 3% when the energy is divided by 2. For the typical absorbance of 25%, the correcting term $\mathrm{Ln}(T_{2f}/T_{2e})$ is about 0.8% and its modulation from the maximum fluence of $170\,mJ/cm^2$ to

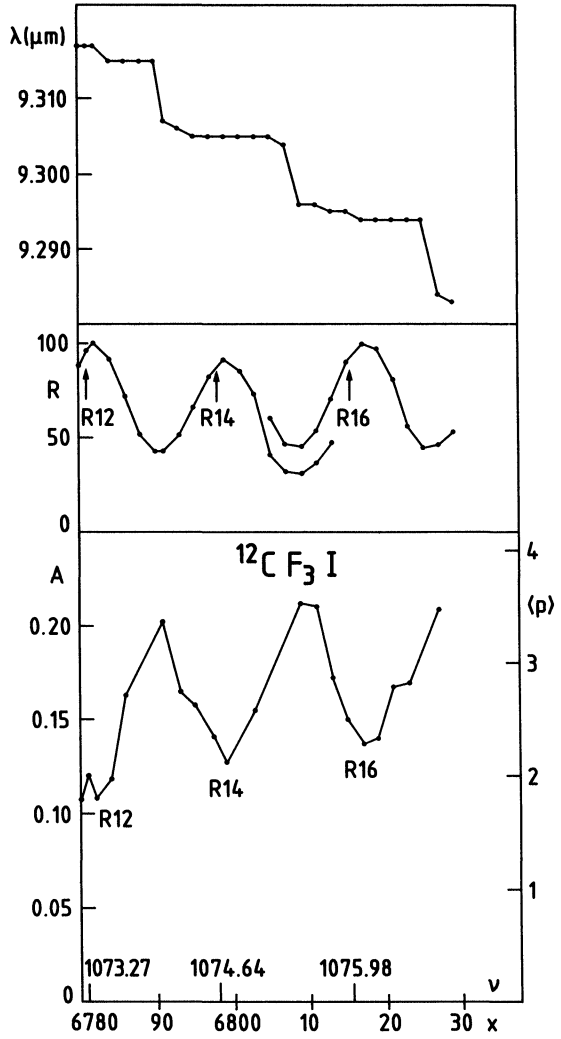

Figure 7 $^{12}CF_3I$ MPA spectrum for laser cavity pressure of 5 Bars. The wavelength λ is plotted in the upper part in μm unit. For other data see Figure 3.

the minimum fluence of 110 mJ/cm^2 does not exceed 0.3%. Then the effect observed is not due to this correction and A_m can be identified to A.

In the most general way, the molecular MPA cross section can be expressed as the following:

$$\sigma(\phi, \nu, f_t, \psi_i) \tag{4}$$

ϕ is the fluence exciting the molecule (J/cm^2); ν is the linecenter frequency of the laser emission; f_t is the electric field temporal evolution for a normalized fluence (obviously f_t is equivalent to the complex spectral distribution f_ν of the electric field); ψ_i is the initial rovibrational state of the molecule.

σ depends on the position of the molecule in the cell through its fluence dependence. But it has been shown that A, and consequently σ, are nearly independent on ϕ at least in the main part of the MPA spectra of $^{12}CF_3I$ and SF_6. Then, $\langle\sigma\rangle = \sigma$ in (1) and the modulation of A cannot be explained by the fluence modulation from 170 to 110 mJ/cm^2 due to the spatial distortion.

Other possible explanations such as self-focusing or defocusing being ruled out by complementary experiments (d), the single remaining cause of the observed modulation lies in the variation of f_t or equivalently f_ν. This explanation is fully consistent with the modulation observed on the laser bandwidth. It must be underlined that this modulation bears on the intensity spectrum $F(\nu) = |f(\nu)|^2$ and not directly on $f(\nu)$. More particularly the observed features are broadening and splitting of $F(\nu)$ in the gain minima. As these features concern frequency scales $\geqslant 0.1\,\text{cm}^{-1}$, the associated time scale is $\leqslant 300$ ps and cannot be observed on $f(t)$ with 1 ns resolution of a photon drag. As it has been checked that no temporal characteristics concerning this last time scale are correlated with the gain curve we can conclude that the effect observed is very likely due to the spectral bandwidth variation and splittings.

However, this simple explanation suffers difficulties coming from the result of Figure 7 and from the complementary experiments (f) and (g) which seem to state a quasi independency between absorbance spectra and variations in laser spectral characteristics. A careful examination of these results shows they are compatible with the bandwidth interpretation if it is assumed that the bandwidth dependence of the absorption is weak for a laser linewidth $\gamma_L < 80\ 10^{-3}\,\text{cm}^{-1}$

or $\gamma_L > 200\ 10^{-3}\ cm^{-1}$ and that the main dependence occurs in the range $[80\text{–}200]\ 10^{-3}\ cm^{-1}$.

A second difficulty comes from the complete absence of molecular features in the spectra reported, for a frequency observation scale $\sim 0.1\text{–}1\ cm^{-1}$. Obviously, there is a smooth variation of the absorbance at a frequency observation scale $>1\ cm^{-1}$, around the strong IR active mode, as it is known for long time from atmospheric CO_2 laser experiments. But no peak assignable to, for example, 2 or 3-photons transitions can be observed. Then, the ν dependence of (4) must be assumed very smooth, i.e. weak for ν varying over $1\text{–}2\ cm^{-1}$. This property of σ is valid within our experimental conditions: the initial distribution of ψ_i is thermal at $T = 295\ K$ and the linewidth range explored is $0.03\ cm^{-1} \leq \gamma_L \leq 0.4\ cm^{-1}$. It results from this analysis that, from one line center to the next, the ν dependence of σ can be ignored, as soon as the ϕ dependence (complementary experiment (a)). There remains only a function $\sigma_T(\gamma_L)$ which explains the variation of A between two successive CO_2 line centers. This function can be extracted from our multiphoton absorption spectra. In the case of SF_6 around the $10P\,20$, the result is reported in Figure 8 (full line). Several

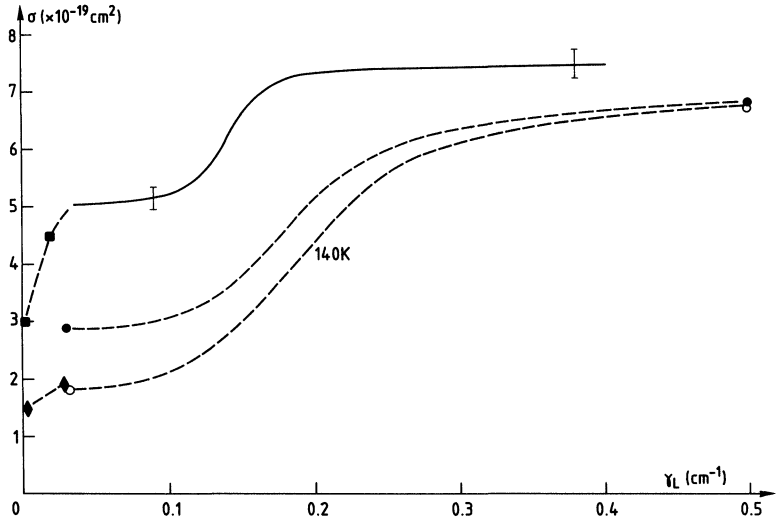

Figure 8 SF_6 MPA cross section around $10P\,20$, versus the laser bandwidth γ_L (in cm^{-1}) at 295 K (full line). Two error bars are indicated. Results of Ref. 4 are also reported at 300 K (black circles) and 140 K (open circles) as soon as those of Ref. 16 (black squares) and 17 (black rhombs). The dashed lines are plotted only to help vision.

points extracted from the works of Refs. 4, 16 and 17 are also reported for comparison and will be discussed in the next section. Our curve settles that σ increases for γ_L around 0.12–0.18 cm^{-1} and that the dependence becomes very flat for $\gamma_L > 0.2$ cm^{-1} which is in agreement with the complementary experiment (f) and (g).

Obviously this result is obtained in an indirect way, since the absorbance variation versus the grating position from one CO_2 line center to the next is interpreted as a bandwidth effect. A direct systematic variation of γ_L for a fixed grating position would be very interesting although practically difficult since numerous gratings with different number of lines per mm, or intracavity beam expanders, should be used.

3. DISCUSSION

3.1. Comparison with similar works

The most comparable MPA experiments reported in the literature are those of Refs. 1, 4, 5 and 9. We will not discuss dissociation experiments performed with high pressure CO_2 lasers because such measurements are much more indirect than absorption.

In Ref. 5 MPA spectra are reported for $^{12}CF_3I$ and CF_3Br. The high pressure laser is identical to our one. Fluences and gas pressures are similar. The main difference with our experiments is the use of an optoacoustic method to measure the energy absorbed. The CF_3I pressure is 0.67 mBar and the fluence 160 mJ/cm^2. The spectrum of $^{12}CF_3I$ is reported on Figure 3 after a linear correction from 160 to 140 mJ/cm^2 in view of improving the comparison (dotted line). The overall features are similar but there are however several differences with our spectrum:

—the absolute value of $\langle p \rangle$ deviates from our one up to ±30% in several parts of the spectrum.

—there is a narrow supplementary peak near 1073.4 cm^{-1} which has no counterpart in our spectrum.

—except this last peak, there is an accurate correspondence between the two spectra in the position of absorption maxima or minima from 9*R* 6 to 9*R* 16 where the absorption is high.

—above the 9*R* 16 line and up to the 9*R* 26, there is also a one to one correspondence between the peaks of the two spectra but with a shift

of about 0.6 cm^{-1} in the position. In this range, there is consequently an "anticorrespondence." Near the 9*R* 24 and 9*R* 26, the correspondence seems to be restored, but the absorption becomes very weak and the peaks of Ref. 5 weakly marked.

We think that these discrepancies can be explained by the different experimental conditions. The optoacoustic method is more indirect than the double ratiometric method and it can be sensitive to spatial distortions of the beam, producing specific modulations. The calibration of the frequency has been made in Ref. 5 using NH_3 absorption, but the reference lines are fairly sparse and a systematic comparison with CO_2 lines is much more preferable. It can be noted that there are no NH_3 reference lines between 1076 and 1084 cm^{-1}[18], i.e. betwen 9*R* 16 and 9*R* 28 where the spectrum of Ref. 5 seems to be shifted from our one. Then, the discrepancy could be a problem of absolute frequency reference. Finally, we have observed in preliminary experiments that irregularities in the laser gas flow could be responsible of frequency jumps. The supplementary peak at 1073.4 cm^{-1} could be due to such an instability.

In Ref. 9, $^{12}CF_3I$ has been reinvestigated with the same device as in Ref. 5. The spectrum obtained at 298 K, 0.13 mBar and 110 mJ/cm^2 is reported on Figure 3 (dashed line). The absolute absorption has been multipled by 0.6 in view of making easier the comparison of the peaks position. In spite of this correction factor, the number of photons absorbed deviate up to 40% from our values in some part of the spectrum. Nevertheless, the peak positions are in almost perfect coincidence, showing without any possible doubt that the structures are exclusively due to a laser effect. Particularly, there is no more peak at 1073.4 cm^{-1}. In Ref. 9, $^{12}CF_3I$ has also been studied at 233 K. The peak positions are unchanged, the absorption being uniformly reduced. Then, such a cooling is insufficient to allow the appearance of molecular features in the $^{12}CF_3I$ spectrum.

We can conclude from these comparisons that either in Ref. 5 or in Ref. 9, a laser bandwidth effect has been observed for $^{12}CF_3I$ without any peak assignable to a specific molecular pathway. Moreover, the spectrum of Ref. 5 is perturbed by several experimental artefacts such as frequency calibration or frequency jumps.

The observation of the $^{12}CF_3Br$ spectrum of the Ref. 5 confirms the correspondence with CO_2 laser lines: from the 9*R* 14 to the 9*R* 30

lines, the absorption minima are located near CO_2 line centers. It seems there is an overall shift of $\sim -0.3\,cm^{-1}$ which could be due to the lack of NH_3 reference lines between $9R$ 16 and $9R$ 28 mentioned above. There are also small modulations, slightly above the experimental uncertainty, superimposed to the main peaks. These substructures could be the manifestation of molecular features but this hypothesis is questionable. Our CF_3Br spectrum has a too small frequency range to allow a detailed comparison but it states the dominant rôle of the laser bandwidth effect for the CF_3Br molecule.

In Ref. 1, the SF_6 MPA spectrum is reported, measurements being performed in an optoacoustic cell cooled at 140 K. The SF_6 pressure is 0.400 mBar and the fluence $270\,mJ/cm^2$. One part of the spectrum is reported on Figure 6 (dashed line, arbitrary unit) but the range explored in Ref. 1 extends up to $950\,cm^{-1}$.

This spectrum shows well defined peaks assigned in Ref. 19, without any correlation with the CO_2 lines. This result seems to contradict our work but there are two main differences which can explain the discrepancy. First, the gas is cooled, which eliminates most hot bands and reduces considerably the number of rotational states. One obvious consequence is that the measured cross-section undergoes a less extensive average over the initial state ψ_i avoiding a smoothing of molecular characteristics. Unfortunately, no spectrum is reported at 300 K. The second and probably more important difference lies in the characteristics of the excitation laser: a telescoping NaCl prism with magnification 6 is introduced in the cavity giving a spectral linewidth of $30\ 10^{-3}\ cm^{-1}$, likely constant whatever be the grating position and much smaller than the linewidth of our laser or that of Refs. 5 and 9. This remark supports the hypothesis of a correlation between the MPA spectrum and the laser bandwidth in our experimental conditions. To the best of our knowledge, the SF_6 MPA spectrum of Ref. 1 is the single one which exhibits evidently molecular structures.

The $\sigma(\gamma_L)$ dependence reported in Figure 8 (full line) can be confirmed and extended by comparison with similar works.

The work of Ref. 4 compares the SF_6 MPA at the $10P$ 20 line center for a narrow bandwidth and a broad bandwidth excitation. The narrow bandwidth excitation is performed at a laser pressure of 4 Bars with a grating and an intracavity beam expander. The broad band excitation uses a 20 Bars laser gas mixture and a NaCl prism. In the former case, the bandwidth is probably $\sim 30.10^{-3}\,cm^{-1}$ while in the latter case, due

to an imperfect antireflection coating, the output coupler acts as a Fabry-Perot and the spectral distribution is formed of a succession of lines distant of $0.208\,cm^{-1}$ and spread over $2\,cm^{-1}$. The sum of the partial f.w.h.m. linewidth is probably about $0.5\,cm^{-1}$. At 300 K and $140\,mJ/cm^2$, the broad band excitation gives a MPA cross section $\sigma = 6.8\ 10^{-19}\ cm^2$ (black circles on Figure 8) while the narrow band excitation gives $\sigma = 2.9\ 10^{-19}\ cm^2$. At 140 K, the MPA cross section is unchanged for the broad band excitation, while it is reduced down to $1.8\ 10^{-19}\ cm^2$ for the narrow band excitation (open circles on Figure 8). Although limited to 2 points, this direct bandwidth variation confirmed the whole aspect of our curve, deduced from the analysis in the previous section. The absolute values are, however, notably different but the experimental conditions also (for example, the SF_6 pressure is 0.23 mBar in the work of Ref. 4). It can be underlined that the broad band excitation has some similarity with multifrequency excitations such as those of Refs. 20 to 23 in which the absorption was also enhanced.

It is now interesting to extend our curve at the low linewidth extremity. This can be done using comparison between single longitudinal mode and conventional multimode excitation. Such a comparison has been performed for TEA lasers, particularly in Ref. 16. The SF_6 MPA cross section has been measured at the $10P\,20$ line center, for 0.47 mBar. At $140\,mJ/cm^2$, the single mode excitation ($\gamma_L \sim 10\,MHz$) gives a MPA cross section $\sigma = 3.0\ 10^{-19}\ cm^2$, while the multimode excitation ($\gamma_L \sim 600\,MHz$) gives $\sigma = 4.5\ 10^{-19}\ cm^2$. This two points are reported on Figure 8 (black squares). Then, there is a rather fast variation of σ from monomode excitation up to $\gamma_L \sim 2\text{–}3\ 10^{-2}\ cm^{-1}$, followed, as demonstrated by our curve, by a flat dependence up to $\gamma_L \sim 8\text{–}9\ 10^{-2}\ cm^{-1}$.

A comparison between monomode and multimode excitation by a TEA laser has been also reported in Ref. 17. The data are plotted in Figure 8 (black rhombs). These points have been obtained at a fluence of $1\,J/cm^2$ and a SF_6 pressure of 0.16 mBar and the comparison with our work is limited, but the relative increase of σ with γ_L is confirmed in the range $\gamma_L \leq 3\ 10^{-2}\ cm^{-1}$.

We can finally comment briefly the difference between the $^{12}CF_3I$ and $^{13}CF_3I$ spectra (Figures 3 and 4) with the help of the spectroscopic data reported in Ref. 12. In $^{12}CF_3I$, a Fermi resonance occurs between ν_1 and $2\nu_5$. As it involves only three vibrational quanta, the coupling is

rather strong, estimated to 2.6 cm^{-1}. Additional $\nu_3 + 3\nu_6$ Fermi resonance seems also present. In $^{13}CF_3I$, the most important Fermi resonance seems to couple ν_1 and $4\nu_6$ with a coupling strength of 0.94 cm^{-1}, involving probably a chain coupling. Then, the number of transitions or their strength is smaller, which explains qualitatively the factor 2 observed between MPA cross sections.

3.2. Interpretation of the MPA cross section curve versus the laser bandwidth

We analyze now quantitatively—although approximately—the result of the Figure 8 showing the dependence of the MPA cross section versus the laser bandwidth γ_L, and particularly the flat dependence occurring for $\gamma_L > 0.2\,cm^{-1}$. When γ_L increases, the excitation can be considered as more and more incoherent. When the excitation is single longitudinal mode $\gamma_L \sim 1/\tau_p$, τ_p being the pulse duration, and the excitation is coherent. Let ν_c be the free spectral range of laser longitudinal modes (ν_c is typically 150 MHz, i.e. 5 10^{-3} cm^{-1}). When $\gamma_L > \nu_c$, the excitation becomes multimode and the longitudinal modes beating occurs giving an irregular intensity evolution with a pseudo period $1/\nu_c$. If the average time τ_a needed to absorb or emit one more photon verifies $\tau_a > 1/\nu_c$ (~7 ns) the structure of the spectral distribution in longitudinal modes can be considered as erased due to the dynamical broadening. Although this condition is fairly critical in the case of our spectra, we want to use it in view of giving a simple semi quantitative explanation to the result.

The coherent excitation of discrete transitions is described by the well known monophoton Rabi frequency:

$$\nu_R = d_{ij,y}E_0/2h \tag{5}$$

or the generalized k-photons Rabi frequency[24]

$$\gamma_{R,k} = \frac{\nu_{R,0\to1}}{\Delta_1} \times \ldots \times \frac{\nu_{R,k-2\to k-1}}{\Delta_{k-1}} \times \nu_{R,k-1\to k} \tag{6}$$

(E_0 is the electric field amplitude, for a linear polarization along $\vec{O_y}$; $d_{ij,y}$ is the dipole matrix element of the $i \to j$ transition, along this axis; Δ_1 is the shift to resonance between the molecular level 1 and 1ν).

The enhancement of the MPA cross section σ from monomode to

multimode excitation can probably be explained in the frame of the coherent excitation scheme by an intensity effect since the maximum intensity is typically doubled by the modes beating, and the relevant E_0 is higher.

In the opposite case of an incoherent excitation, the molecular distribution evolution can be described by rate equations using Einstein coefficients.[25]

Let $F_L(\nu)$ be the normalized laser emission spectrum ($\int d\nu F_L(\nu) = 1$), its maximum being in $\bar{\nu}$; γ_L its f.w.h.m.; ν_{ij} the frequency fo the discrete transition $i \rightarrow j$. For a discrete monophoton transition around or not too far from resonance, i.e. if $|\bar{\nu} - \nu_{ij}| \lesssim \gamma_L$, the absorption cross section is given by:

$$\sigma_{i\rightarrow j} = \sum_{i\rightarrow j} \nu F_L(\nu_{ij}) \tag{7a}$$

with:

$$\sum_{i\rightarrow j} = \frac{4\pi^2}{3} \frac{|d_{ij}|^{2\downarrow}}{4\pi\varepsilon_0 \hbar c} \tag{7b}$$

If the excitation is close to resonance, $F_L(\nu_{ij}) \sim 1/\gamma_L$ and the absorption rate can be expressed:

$$Z_{i\rightarrow j} \simeq 4\pi^2 \nu_R{}^2/\gamma_L \tag{8}$$

A transition rate can be also defined for a k-photons transition with the upper level around resonance, the intermediate steps being off resonance:

$$Z_{i\rightarrow j} \simeq 4\pi^2 |\gamma_{R,k}|^2/\gamma_L \tag{9}$$

The condition for which the excitation must be considered as incoherent is:

$$\gamma_L > 2\pi\nu_R \quad \text{or} \quad 2\pi\gamma_{R,k} \tag{10}$$

Formulas (7) to (10) allow a first qualitative understanding of the γ_L dependence: at resonance, when γ_L increases, the cross section diminishes; off but not too far from resonance, the cross section is enhanced since $F_L(\nu_{ij})$ grows with ν_L. The enhancement of σ with γ_L from 8 to 20 10^{-2} cm^{-1} for a fixed frequency ν means that transitions detuned from ν of $\sim$0.1–0.2 cm^{-1} becomes active because γ_L approaches this typical detuning. Then, we must admit that there is a background of transitions having this typical spacing $\delta_m \sim 0.1$–$0.2\,\text{cm}^{-1}$.

When γ_L exceeds this value δ_m, the transitions can no more be considered as discrete and they act as a quasi-continuum (relatively to the laser linewidth). A Fermi Golden Rule is therefore valid and the absorption cross section is given by:

$$\sigma_{i\to i+h\nu} = \sum_0 \nu F_m(\nu) \tag{11a}$$

with

$$\sum_0 = \frac{4\pi^2}{3}\frac{\bar{d}^2}{4\pi\varepsilon_0 c\hbar} \tag{11b}$$

$F_m(\nu)$ is the normalized distribution of the oscillator strength borne by the transitions acting as a quasi-continuum ($\int d\nu F_m(\nu) = 1$) $\bar{d}$ is the dipole transition moment corresponding to this oscillator strength.

Formulas (11) explain the most remarkable feature of the curve in Figure 8: the flat dependence for $\gamma_L > \delta_m \sim 0.1$–$0.2\,\mathrm{cm}^{-1}$: σ does not depend anymore on γ_L as it is known for Fermi Golden Rule rates. Moreover, the smooth dependence of σ versus ν from one CO_2 line to the next results from the f.w.h.m. of F_m which is typically $\Gamma_m \sim 10\,\mathrm{cm}^{-1}$. It must be kept in mind that formula (11) are valid only if $\gamma L < \Gamma_m$ but the range explored in Figure 8 is far from this limit which would be reached only by lamps.

One can find a paradox in the total absence of fine molecular resonances in our MPA spectra, although γ_L is smaller than the typical spacing δ_m for successive ranges of about $0.8\,\mathrm{cm}^{-1}$ around each line center. As discussed above, the average over the initial state ψ_i can erase these structures. Second, for a given ψ_i, the cross section σ is also an average over the successive photons absorbed. The slowest steps enforce the excitation rate, i.e., precisely the off resonant steps. Third, for a given ψ_i there is also an average over different possible excitation pathways.

We can now apply the formulas (11) in the limit of quasi-continuous transitions ($\gamma > \delta_m$) assuming that all the oscillator strength of the IR active mode is borne by these quasi-continuous transitions. For $^{12}CF_3I$, $\bar{d} = 0.39D$,[26] $\nu = 1075\ \mathrm{cm}^{-1}$. Around resonance with the ν_1 mode $F_m(\nu) \sim 1/\Gamma_m$, with $\Gamma_m \sim 10\ \mathrm{cm}^{-1}$, which gives $\sigma \sim 6\ 10^{-18}\ \mathrm{cm}^2$. This result exceeds of a factor 40 the maximum experimental MPA cross section measured ($\sim 1.5\ 10^{-19}\ \mathrm{cm}^2$). It is clear that the quasi-

continuous transitions bear only a small part of the total oscillator strength, i.e. less than 1/40. This is fully consistent with the fact that the strong PQR transitions bearing the most important part of the oscillator strength have a typical spacing in the range 1–3 cm^{-1}, and not 0.1–0.2 cm^{-1}. We are therefore lead to the conclusion that aside these strong transitions there exists a background of weak transitions bearing about $\varepsilon = 1$–2% of the total oscillator strength, with a typical spacing $\delta_m = 0.1$–$0.2\,cm^{-1}$ and spread over $\Gamma_m \sim 10\,cm^{-1}$. Then, each weak transition bears about 1/4500 of the total oscillator strength. For $\phi = 140\,mJ/cm^2$, $\tau_p = 45$ ns, $\vec{d} = 0.39D$, we obtain for each weak transition a typical Rabi frequency $\nu_{Ri\to j} \sim 2.5\ 10^{-3}\ cm^{-1}$ (75 MHz). This value is consistent with the condition (10) in the range explored. Moreover, it means that even in the coherent case, weak transitions can play a non negligible rôle: a fraction $4\nu_R/\delta_m$ of the molecules can be considered around resonance for weak monophoton transitions in the coherent case, i.e. ~10%. Two photons weak transitions can also play a rôle in the coherent case for a 45 ns pulse. Finally, the formula (6) indicates that an intermediate weak transition with a Rabi frequency $2.5\ 10^{-3}\ cm^{-1}$ and a detuning $2.5\ 10^{-2}\ cm^{-1}$ can help a coherent k-photons transition more effectively than an intermediate strong transition for which $\nu_R \sim 0.1\ cm^{-1}$ and the detuning is greater than $1\,cm^{-1}$.

If this interpretation of the curve in Figure 8 is correct we obtain quantitatively, for the first time to the best of our knowledge, the rough characteristsics of the weak rovibrational transitions. Their importance has been mentioned only in a few works. In Ref. 27, an analytical treatment of them has been developed, but without discussing the rôle of the laser bandwidth. The most interesting question concerns the nature of these weak transitions. For spherical tops molecules such as SF_6, $\Delta R \neq 0$[28] and $\Delta n \neq 0$[29] transitions have been evoked. Whatever be the molecule, $|\Delta j| > 1$ transitions[29] are also possible but can be understood as k-photons transitions. It has been also recently suggested in the interpretation of Raman probing of the vibrational distribution[30,31] that the MPA process could involve combination bands. We think their rôle could be important in MPA experiments and particularly for broad band excitations and they deserve more careful attention.

The vibrational ladder is commonly shared in two parts: a lower part of separated modes and an upper part of redistributed states—the

quasi-continuum. But the couplings responsible of the redistribution for sufficiently high energies can be important at lower energies by perturbing the pure modes. Then, if an arbitrary mode combination $|(v_i)\rangle$ and a state of the pure absorbing mode ladder $|0, v_a, 0\rangle$ are quasi-coincident in energy, the former is perturbed and becomes:

$$|(v_i)\rangle + \frac{V_{ia}}{\Delta E} |0, v_a, 0\rangle \tag{12}$$

The perturbation gives now a weak dipole matrix element wth the state $|0, v_a-1, 0\rangle$ of the pure absorbing mode ladder and the molecule can leave this one during the interaction. It can be noticed that the transition occurs through the absorbing mode dipole component, which means that the weak transitions remain clustered around the absorbing mode, although the molecule leaves it. For a typical spacing $\Delta E \sim 1\,\text{cm}^{-1}$ the state of formula (12) can bear 1/4500 of the oscillator strength if $V_{ia} \sim \Delta E/\sqrt{45000}$, i.e.: $V_{ia} \sim 1.5\ 10^{-2}\ \text{cm}^{-1}$. Then, small intramolecular couplings can explain efficient absorption towards mode combinations. In SF_6, for example, the vibrational density of states is $1.6/\text{cm}^{-1}$ at 2 photons.[32] As the rotational states multiply this value by several tens, weak transitions of this type can be present since the second photon absorbed. Above the onset of the quasi continuum, the oscillator strength is largely redistributed, although on a rather narrow frequency range of $1\text{–}10\,\text{cm}^{-1}$ as shown in Refs. 26 or 33.

We can conclude this analysis of the bandwidth effect by several remarks:

—in Ref. 4 an analogy was suggested between the bandwidth effect and the intensity effect reported in Ref. 34 for subnanosecond pulses. This analogy lies on an assumed similarity between γ_L and ν_R. Although the explanation can be practically correct, the molecular field interaction is in fact very different.

—the incoherence of the field has been treated here in an oversimplified way, although, especially for lasers, non trivial situations can be involved.[35–37]

—the laser characteristics could have consequences on the absorption not only through the linewidth but also through the temporal pulse shape if some effects analogous to a transition from adiabatic to sudden switching of the light occur.[38–41]

—the existence of a background of weak, but dense, resonances extended over several cm^{-1} can explain the result of Refs. 42 and 43 in which rotational levels were shown to be depopulated for excitations largely detuned with the low intensity absorption spectrum.

4. CONCLUSION

The most important result of this work is the correlation between MPA spectra and CO_2 laser lines. Careful examination of the literature leads to the conclusion that MPA spectra performed with high pressure CO_2 lasers without other selective element than a grating exhibit the same correlation. The most probable interpretation involves a laser bandwidth effect. The complete and semi-quantitative understanding of the data seems only possible if the existence of a background of weak transitions typically spaces of $0.1\ cm^{-1}$ and bearing a few percent of the total oscillator strength is assumed between the ground state and the beginning of the quasi-continuum.

The probable rôle of the laser bandwidth shows that it would be highly desirable to perform MPA spectra with single longitudinal mode (SLM) high pressure CO_2 lasers. Such a source is difficult to realise. Very recently, SLM pulses of about 100 mJ have been reported for CO_2 HPL using different intracavity dispersive elements.[44,45] Another possible method is the injection of a continuously tunable source, which allows energies higher than 300 mJ. This method has been also recently tested and analysed.[46]

Only such experiments are able to put in evidence without ambiguity the MPA rovibrational pathways, with the important additional advantage to conciliate experimental works and theoretical computations, the last being only accessible for coherent excitations.

Acknowledgements

We are grateful to Dr. Ph. Millié for critical reading of the manuscript and to Drs. M. Gilbert, P. Isnard and G. Salvetat for providing the Optical Multichannel Analyzer.

References

1. S. S. Alimpiev *et al.*, *Opt. Com.* **31**, 309 (1979).
2. S. S. Alimpiev *et al.*, CLEO Conf. Washington DC, USA (June 1981).

3. S. S. Alimpiev *et al.*, *Sov. J. Quant. Electr.* **13**, 331 (1983).
4. S. S. Alimpiev *et al.*, *Appl. Phys. B,* **35**, 1 (1984).
5. E. Borsella *et al.*, *Chem. Phys. Lett.* **101**, 86 (1983).
6. A. Giardini-Guidoni, E. Borsella and R. Fantoni, *Gazz. Chim. It.* **113**, 635 (1983).
7. M. Snels *et al.*, Laser Processing and Diagnostics Conf., University of Linz, Austria (July 1984).
8. M. Snels *et al.*, *Chem. Phys. Lett.* **122**, 480 (1985).
9. U. Del Bello *et al.*, *Chem. Phys. Lett.* **114**, 467 (1985).
10. V. N. Bagratashvili *et al.*, *Opt. Com.* **38**, 31 (1981).
11. C. Angelié and R. Capitini, *Applied Optics* **26**, (1987).
12. H. Bürger *et al.*, *Molec. Phys.* **55**, 255 (1985).
13. M. Cauchetier *et al.*, Note CEA n° 2348 (May 1983).
14. A. V. Nowak and D. O. Ham, *Opt. Lett.* **6**, 185 (1981).
15. J. R. Ackerhalt, H. W. Galbraith and J. C. Goldstein, *Opt. Lett.* **6**, 377 (1981).
16. J. L. Lyman, B. J. Feldman and R. A. Fisher, *Opt. Com.* **25**, 391 (1978).
17. J. G. Black *et al.*, *Phys. Rev. A,* **19**, 704 (1979).
18. A. R. H. Cole, Table of wavenumbers for the calibration of IR spectrometers. Pergamon Press (Oxford, New York, 1985).
19. M. Dilonardo, M. Capitelli and C. D. Cantrell, *Appl. Phys. B,* **29**, 181 (1982).
20. A. V. Evseev and A. A. Puretzky, *Laser Chem.* **5**, 167 (1985).
21. V. M. Apatin, V. N. Lokhman and G. N. Makarov, *Laser Chem.* **5**, 231 (1985).
22. A. V. Evseev, V. S. Letokhov and A. A. Puretzky, *Appl. Phys. B,* **36**, 93 (1985).
23. A. V. Evseev and A. A. Puretzky, *Sov. J. Quant. Electr.* **15**, 689 (1985).
24. D. M. Larsen and N. Bloembergen, *Opt. Com.* **17**, 254 (1976).
25. J. Dupont-Roc, Proceedings of the Summer School on Chemical Photophysics, Les Houches (1979) (Ed. du CNRS, Paris, 1979), p. 31.
26. V. N. Bagratashvili *et al.*, *Sov. Phys. JETP,* **50**, 1075 (1979).
27. V. M. Akulin, *Sov. Phys. JETP,* **56**, 533 (1982).
28. I. N. Knyazev, V. S. Letokhov and V. V. Lobko, *Opt. Com.* **25**, 337 (1978).
29. V. N. Bagratashvili *et al.*, Multiple photon IR laser photophysics and photochemistry, Harwood Academic Publisher (London, Paris, New York, 1986).
30. Yu. S. Doljikov *et al.*, *Chem. Phys. Lett.* **124**, 304 (1986).
31. V. S. Doljikov *et al.*, *Chem. Phys.* **102**, 155 (1986).
32. E. Thiele, J. Stone and M. F. Goodman, *Chem. Phys. Lett.* **76**, 579 (1980).
33. C. Angelié and P. Millié, *Chem. Phys.* **82**, 171 (1983).
34. H. S. Kwok, E. Yablonovitch and N. Bloembergen, *Phys. Rev. A,* **23**, 3094 (1981).
35. J. R. Ackerhalt, H. W. Galbraith and P. W. Miloni, *Phys. Rev. Lett.* **51**, 1259 (1983).
36. I. Shek and J. Jortner, (a) *J. Chem. Phys.* **81**, 4858 (1984). (b) *Chem. Phys.* **97**, 1 (1985). (c) *Chem. Phys.* **106**, 179 (1986).
37. K. Wodkiewicz and J. H. Eberly, *J. Opt. Soc. Am. B,* **3**, 628 (1986).
38. G. L. Peterson and C. D. Cantrell, *Phys. Rev. A,* **31**, 807 (1985).
39. J. Oreg, F. T. Hioe and J. H. Eberly, *Phys. Rev. A,* **29**, 690 (1984).
40. V. Yu. Finkel'shtein, *Sov. Phys. JETP,* **61**, 912 (1985).
41. E. Kyrola, *J. Opt. Soc. Am. B,* **3**, 453 (1986).
42. V. M. Apatin *et al.*, *Opt. Com.* **47**, 251 (1983).
43. V. M. Apatin *et al.*, *JETP Lett.* **37**, 432 (1983).
44. B. K. Deka, M. A. Rob and J. R. Izatt, *Opt. Com.* **57**, 111 (1986).
45. G. Kovar, M. Piche and P. A. Belanger, SPIE Proceedings, Québec (1986).
46. C. Angelié, R. Capitini and P. Girard, *Applied Optics* **26**, (1987).